Adv Polym Sci (2008) 212: 49–84
DOI 10.1007/12_2008_144

Published online: 8 May 2008

Polyfluorenes for Device Applications

Show-An Chen (✉) · Hsin-Hung Lu · Chih-Wei Huang

Chemical Engineering Department, National Tsing-Hua University,
30013 Hsinchu, Taiwan, Republic of China
sachen@che.nthu.edu.tw

1 Introduction 51

2 Concepts for Performance Improvement of Polyfluorene Devices 51
2.1 Background of Electronic States of PFs 51
2.2 Adjustment of Chain Structures in PFs 54
2.2.1 Chemical Modifications 54
2.2.2 Physical Manipulation 63
2.3 Sources of Undesirable Green Emission in PF-based PLEDs 64

3 PFs with Various Emission Colors 65
3.1 Green and Red Emitters 65
3.1.1 Chemical Strategy via Fluorescent Moiety Incorporated in Polymer Backbone, Side Chain, or Chain End 65
3.1.2 Chemical Strategy via Phosphorescent Moiety Incorporated in Polymer Side Chain and Backbone 70
3.2 White Emitters 72
3.2.1 Physical Blending System 72
3.2.2 Chemical Strategy: Single-Polymer Approach 73

4 Alteration of Interfaces Between PFs and Electrodes 75
4.1 Hole-Transporting Layer 75
4.2 Cathode Materials and Electron-Injection/Hole-Blocking Layer 78

5 Summary 81

References 82

Abstract This article mainly reviews the approaches that have been proposed to improve the device performance of polyfluorene (PF)-based polymer light-emitting diodes (PLEDs). Chemical modifications on main chains, side chains, and chain ends of PFs via the incorporation of charge-transport moieties can reduce the hole- and electron-injection barriers; while physical manipulation on main-chain structures of PFs, poly(9,9-di-*n*-octylfluorene) (PFO), after dipping in mixed solvent/non-solvent (tetrahydrofuran/methanol) can generate β-phase with extended conjugation length, leading to a promoted charge balance and stable pure blue emission. Hole- and electron-injection barriers can be effectively lowered by the insertion of hole-transport and electron-injection layers, respectively. The recent development of PFs with various emission colors, via physical blending or chemical modification, are presented for a comprehensive understanding of PFs for device applications. The deliberate choice of cathode material with work function matching the lowest unoccupied molecular orbital (LUMO) levels of PFs is another efficient method for increasing electron flux, and is also discussed in this review.

Keywords Device performance · Electron-transport moiety · Hole-transport moiety · Polyfluorenes · Polymer light-emitting diode

Abbreviations

Alq_3	Tris-(8-hydroxyquinoline) aluminum
$Ca(acac)_2$	Calcium acetylacetonate
CIE	Commission Internationale de l'Eclairage
CN	Cyano
CV	Cyclic voltammetry
Cz	Carbazole
DBT	4,7-Di-2-thienyl-2,1,3-benzothiadiazole
DOF	9,9-Dioctylfluorene
E	Electric-field
Ea	Electron affinity
Eg	Optical gap energy
EL	Electroluminescence
ETM	Electron-transport moiety
F-TBB	1,3,5-Tris-(4′-fluorobiphenyl-4-yl)benzene
FETs	Field-effect transistors
FI	Electric field induction
HOMO	Highest occupied molecular orbital
HTL	Hole-transport layer
HTM	Hole-transport moiety
Ip	Ionization potential
ITO	Indium tin oxide
LEDs	Light-emitting diodes
LUMO	Lowest unoccupied molecular orbital
NTSC	National Television System Committee
OCz	9-Octylcarbazole
OXD	Oxidazole
PEDOT:PSS	Poly(styrene sulfonic acid)-doped poly(3,4-ethylenedioxy-thiophene)
PEO20	PEO doped with 20 wt. % Cs_2CO_3
PFO	Poly(9,9-di-*n*-octylfluorene)
PFs	Polyfluorenes
PLED	Polymer light-emitting diode
PLQEs	Photoluminescence quantum efficiencies
poly-TPD	Polymeric triphenyldiamine derivative
PVK	Poly(*N*-vinylcarbazole)
SAM	Self-assembly monolayer
SPF	Spiropolyfluorene
TAA	Triarylamine
TAZ	Triazole
TOF	Time-of-flight
TPA	Triphenylamine
TPBI	1,3,5-Tris-(*N*-phenylbenzimidazol-2-yl)benzene
TPD-Si_2	4,4′-Bis[(*p*-trichlorosilylpropylphenyl)phenylamino]biphenyl
TSC	Thermally stimulated current
UV	Ultraviolet-visible
V_{bi}	Built-in voltage

η_e	Fraction of emitted photons that pass out of the device
η_r	Fraction of electron/hole pairs that recombine to form excitons
μ_p	Hole mobility
Φ_{EL}	External EL quantum efficiency
Φ_{PL}	Photoluminescent efficiency
χ	Fraction of hole-electron recombinations resulting in singlet excitons
$(FO)_n$	Oligo(9,9-dioctylfluorenyl-2,7-diyl)

1 Introduction

The applications of conjugated polymers in light-emitting diodes (LEDs) [1, 2], field-effect transistors (FETs) [3, 4], and plastic solar cells [5, 6] have attracted great attention recently. In polymer light-emitting diodes (PLEDs), polyfluorenes (PFs) are promising candidates as blue emitters due to their high photoluminescence quantum efficiencies (PLQEs) as solid films [7], their excellent solubility and film-forming ability, and the ease of controlling their properties via facile substitution in the 9,9-position of the fluorene unit [8–10]. In addition, chemical modifications on main chain, side chain, and chain end of PFs allow elaborate tuning of emission color covering the whole visible range (blue, green, yellow, red, and white), enhancement of device performance, and improvement of long-term operational stability. On the other hand, various types of chain conformation and chain stacking of PFs permit relatively easy physical manipulation for identical purposes as the chemical methods. In this review, we focus on the application of PFs in electroluminescent devices and reveal approaches for an enhancement of device performance. The basic electronic properties of PFs are first introduced to give a guideline on the effects of chemical modification and physical manipulation of PF structure on device performance. After that, we review the recent developments of PFs with various emission colors for a comprehensive understanding of PFs in device applications. Finally, the topic of alteration of the interface between PF and electrode is discussed.

2 Concepts for Performance Improvement of Polyfluorene Devices

2.1 Background of Electronic States of PFs

The fundamental properties of electronic states include energy levels of the highest occupied molecular orbital (HOMO) and lowest unoccupied molecular orbital (LUMO) as well as mobilities of hole and electron carriers. These

allow one to identify the minor charge carrier in PFs so that a strategy can be planned for promoting device performance. The factors governing the fluorescent external electroluminescence (EL) quantum efficiency Φ_{EL} can be depicted by the equation,$\Phi_{EL} = \eta_r \chi \Phi_{PL} \eta_e$ [11], where η_r is the fraction of electron/hole pairs that recombine to form excitons, χ the fraction of hole–electron recombinations resulting in singlet excitons, Φ_{PL} the photoluminescent efficiency, and η_e the fraction of emitted photons that passes out of the device. However, χ can be promoted to a higher value in cases where: (1) triplet excitons so generated can be recovered to become emissive in the visible light region, and (2) charge trapping and/or energy transfer occur in multiple emissive species system.

For poly(9,9-di-*n*-octylfluorene) (PFO), which is deemed a model polymer in PFs, Janietz and coworkers reported its HOMO (equivalent to ionization potential, Ip) and LUMO (equivalent to electron affinity, Ea) levels as 5.8 and 2.12 eV below the vacuum level, respectively, as determined from cyclic voltammetry (CV) measurements of PFO thin solid film [11] as shown in Fig. 1a. However, the HOMO and LUMO levels provide a larger band gap of 3.68 eV than the value of 2.95 eV determined from the onset position in the ultraviolet-visible (UV) absorption spectrum of PFO film. If the band gap is taken as 2.95 eV and the HOMO level as 5.8 eV, the LUMO level of PFO

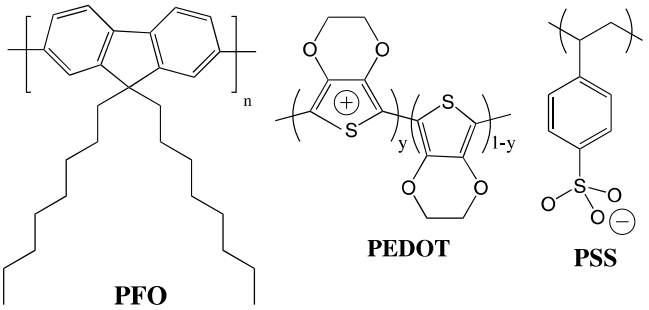

can be determined as 2.85 eV, quite close to the work function of a calcium electrode (2.9 eV). They recommended the use of the LUMO level determined by CV measurement (2.12 eV) because current density–electric field data exhibit an injection-limited nature for the device with a configuration of indium tin oxide (ITO)/PFO/Ca. But, this is still a controversial issue because, as shown in Fig. 1b, the hole-only current [ITO/poly(styrene sulfonic acid)-doped poly(3,4-ethylenedioxy-thiophene) (PEDOT:PSS)/PFO/Au] is two to three orders of magnitude smaller than the electron-only current (ITO/Ag/PFO/Ca) reported by Boudenbergh et al. [13], implying that a LUMO value of 2.85 eV seems more accurate because this value (very close to the

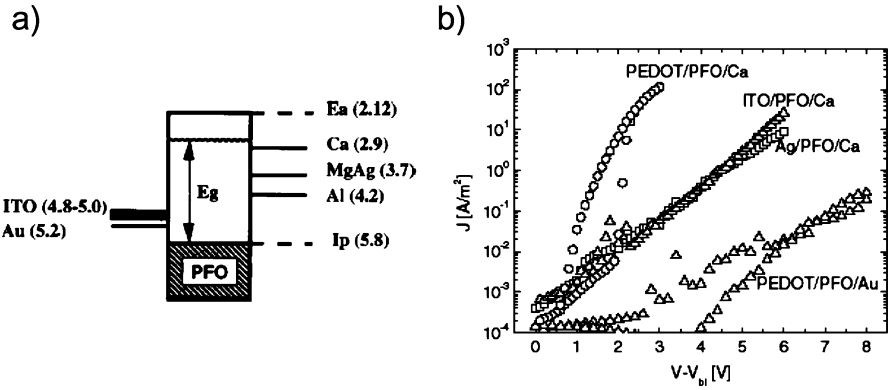

Fig. 1 **a** Schematic diagram showing the Ip and Ea values of PFO relative to the work functions of common electrode materials used in PLEDs. The figures in *brackets* are the respective energies in eV. The optical gap energy E_g (2.95 eV) is also shown (taken from [12]). **b** Current density–voltage characteristics of a PEDOT/PFO/Au (hole-only device) and Ag/PFO/Ca (electron-only device). Bipolar device of ITO/PFO/Ca and PEDOT/PFO/Ca are also shown (taken from [13]). Note that *PEDOT* is the abbreviation of PEDOT:PSS here

work function of the Ca cathode) can generate a negligible electron-injection barrier to cause the observed larger electron current.

Bradley and coworkers reported the hole mobility of PFO to range from 3×10^{-4} to 4.2×10^{-4} $cm^2\,V^{-1}\,s^{-1}$ for an electric field ranging from 4×10^4 to 5×10^5 $V\,cm^{-1}$ (see Fig. 2a) via the thick-film ($\sim$3 μm) time-of-flight (TOF) technique [14]. Meanwhile, PFO film after alignment on polyimide film (pre-

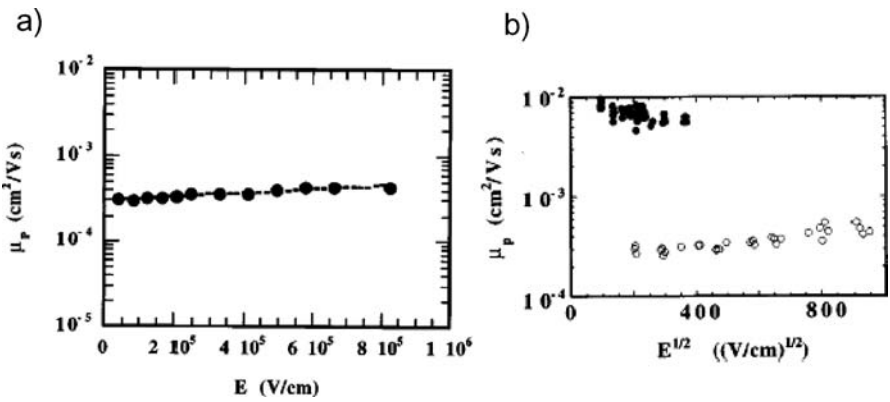

Fig. 2 **a** Field dependence of the hole mobility (μ_p) in spin-coated PFO film at 300 K (taken from [14]). **b** Field dependence of the room-temperature hole mobilities for an aligned, quenched PFO film (*filled circles*) and for an isotropic spin-coated PFO film (*empty circles*) (taken from [15])

viously rubbed by nylon cloth) under thermal annealing at 200 °C gives a higher hole mobility of 5×10^{-3} to 9×10^{-3} $cm^2\ V^{-1}\ s^{-1}$ for electric fields of 1.6×10^5 to 1×10^4 $V\ cm^{-1}$ than isotropic PFO film, as shown in Fig. 2b [15]. On the other hand, electron mobility of PFs was scarcely reported due to the dispersive nature of electron current versus time in TOF measurements [14]. However, based on the configuration of FET, Friend and coworkers reported the electron mobility of PFO as 5×10^{-3} $cm^2\ V^{-1}\ s^{-1}$, which is almost one order higher than its hole mobility of 3×10^{-4} $cm^2\ V^{-1}\ s^{-1}$, also measured by the configuration of FET [16].

2.2 Adjustment of Chain Structures in PFs

2.2.1 Chemical Modifications

In this section, we review the effects of structure modifications for PFs with alkyl and aryl side chains or with charge-transport moieties on device performance. Spiropolyfluorenes (SPFs) having the structure of two phenylene units perpendicularly connected by a tetrahedrally bonded carbon atom are also discussed.

2.2.1.1 PFs with Alkyl and Aryl Side Chains

The first single-layer PF-based PLED with polymer **1** as emitting layer was reported by Yoshino and coworkers [17]. For this device with ITO and magnesium–indium alloy (Mg:In) as anode and cathode, respectively, its main EL emission peak locates at 470 nm, but no data on efficiency was given. However, the authors pointed out that electron injection is difficult because of the large energy barrier (1 eV) between **1** (LUMO 2.9 eV) and the Mg:In cathode (work function of Mg 3.9 eV), while the hole-injection barrier [0.2 eV, as estimated from the work function of ITO (5.5 eV) and the HOMO level of **1** (5.7 eV)] is relatively low as compared to the electron-injection barrier (1 eV). Bradley and coworkers reported that the device with PFO as emit-

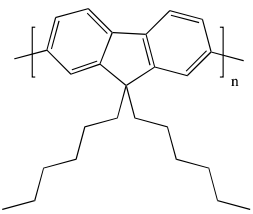

1

ting layer (200 nm) and polymeric triphenyldiamine derivative (poly-TPD, 60 nm) as hole-transport layer (HTL) exhibits a blue emission with the main peak at 436 nm and reaches a luminance of 600 cd m^{-2} and current efficiency of 0.25 cd A^{-1} at the drive voltage 20 V [18]. The incorporation of poly-TPD (HOMO 5.28 eV) in the device introduces a new step in between ITO (work function 5 eV) and PFO (HOMO 5.8 eV) for better hole injection.

Carter and coworkers studied how side-chain branching in PFs affects device performance with and without an additional HTL of cross-linkable polymer **2** [19]. They found that the device efficiency is affected more by the position of the exciton recombination zone than by variations of polymer morphology induced by side-chain branching, which mainly controls the relative emission between vibrational energy levels and has a minimal effect on polymer charge transport properties. For double-layer devices (ITO/PEDOT:PSS/**2**/**3**, **4**, or **5**/Ca), a typical brightness of 100 cd m^{-2} at 0.8 MV cm^{-1}, maximum luminance of 10 000 cd m^{-2} at 1.5 MV cm^{-1}, and device efficiencies between 1.3 and 1.8 cd A^{-1} for **3** and **5** branching can be achieved.

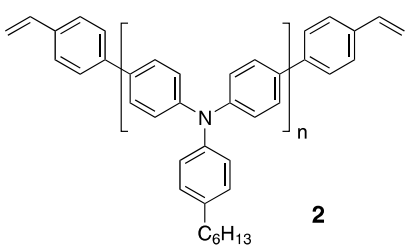

2

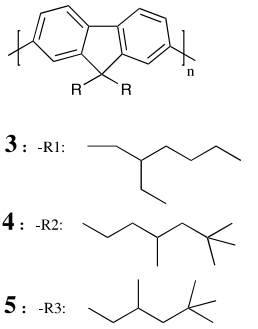

Lee and Hwang synthesized a PF with aryl side chains **6** via the Yamamoto coupling reaction [20]. The device fabricated therewith (ITO/PEDOT:PSS/**6**/Ca/Al) emits blue light with suppressed long tail emission but gives low performance with maximum efficiency of 0.03 cd A^{-1} and maximum luminance of 820 cd m^{-2}. Note that the device could bear considerably high current density (>1.5 A cm^{-2}).

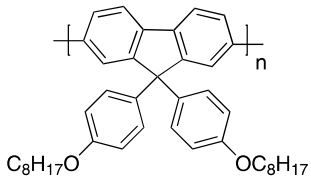

6

Yu et al. first reported the introduction of spiro links onto part of the PF backbone [21]. The resulting spiro-funcationalized PF copolymer, **7**, exhibits narrower EL emission spectra than polyalkylfluorene and the device [ITO/PEDOT:PSS/poly(*N*-vinylcarbazole) (PVK)/**7**/Ca/Al] exhibits low efficiency (0.54%), low luminance (15 cd m^{-2}), and high turn-on voltage (7 V). However, the full SPF, **8**, synthesized using an AB-type monomer via Suzuki coupling gives no apparent green emission, even after heat treatment, though no device performance data were provided [22]. Another SPF with branched dialkyl side chains, **9**, prepared by Vak et al. [23] was found to give pure blue emission with Commission Internationale de l'Eclairage (CIE) coordinates (0.17, 0.12) from the device ITO/PEDOT:PSS/**9**/ LiF/Ca/Ag and exhibited a turn-on voltage of 6 V, maximum luminance of 1600 cd m^{-2} and external quantum efficiency of 0.20% (0.19 cd A^{-1}).

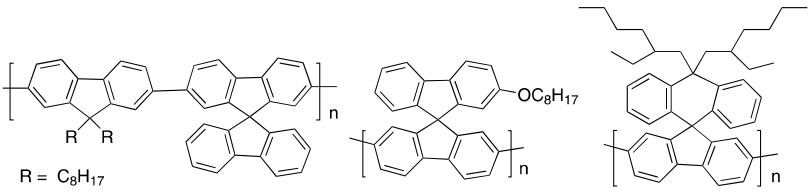

7 **8** **9**

2.2.1.2 Incorporation of Hole-Transport Moiety (HTM)

To obtain better device performance, achieving charge balance in PLED is crucial. The imbalance in charge carriers is due to the high barrier for hole injection and the discrepancy in charge carrier mobilities. Therefore, facilitating hole injection via introducing HTMs onto the PFs would be the key factor to improve the device performance.

Meerholz and coworkers incorporated the HTM (triphenyldiamine derivative) into the backbone of SPF to elevate the device efficiency through promoting hole injection/transport properties [24]. The cross-linkable oxetane-functionalized SPF derivatives **10–12** were also synthesized to realize full color display via spin-coating processes. The resulting EL devices (ITO/PEDOT:PSS/**10**, **11**, or **12**/Ca/Ag) showed maximum efficiencies of 2.9, 7.0, and 1.0 cd A^{-1} for blue, green, and red emissions, respectively.

Li et al. synthesized an alternating 9,9-dioctylfluorene/9-octylcarbazole (DOF/OCz) copolymer **13** with a (DOF:OCz) molar ratio of 3:1 [25]. The device [ITO/**13**/1,3,5-tris-(4′-fluorobiphenyl-4-yl)benzene (F-TBB)/tris-(8-hydroxyquinoline) aluminum (Alq_3)/LiF/Al, where F-TBB and Alq_3 are hole-blocking and electron-transport layers, respectively] exhibits maximum device luminance of 350 cd m^{-2} (27 V) and luminance efficiency of 0.72 cd A^{-1} at a practical brightness of 100 cd m^{-2}. The results are better than those

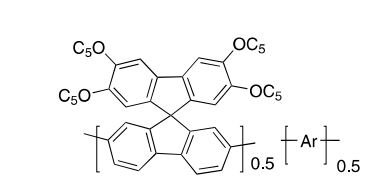

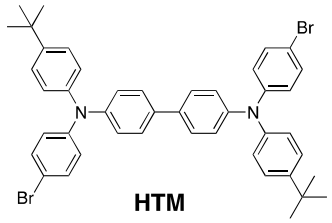

10 (blue), Ar: 15% (B1)/ 25% (B2)/ 10% (HTM)
11 (green), Ar: 25% (B2)/ 15% (G1)/ 10% (HTM)
12 (red), Ar: 25% (B2)/ 10% (G2)/ 5% (R1)/ 10% (HTM)

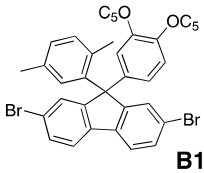

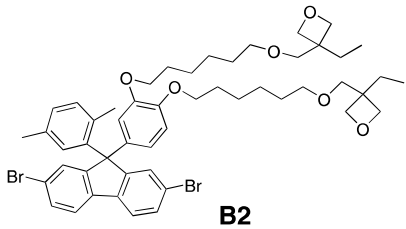

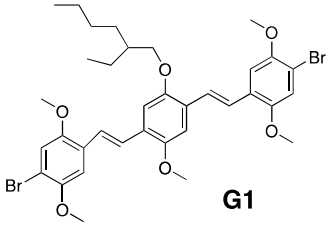

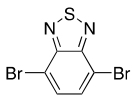

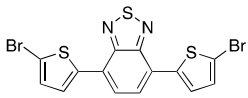

of the PFO-based device (maximum device luminance and luminance efficiency were 160 cd m^{-2} at 27 V and 0.30 cd A^{-1} at 100 cd m^{-2}, respectively). The higher device performance of **13** is attributed to a more efficient hole injection from the ITO anode into the emitting layer because the HOMO level of **13** is reduced to 5.39 eV and is closer to the ITO work function (4.8 eV) than PFO (HOMO level 5.63 eV). On the other hand, the **13**-based device emits blue light with two vibronic peaks at 423 and 443 nm and a low intensity in the region of 500–600 nm.

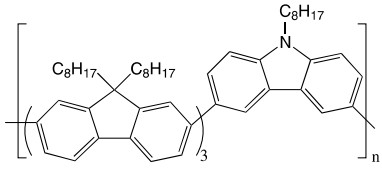

13

For the case of PFs with HTM on the side chain, the incorporation of triphenylamine (TPA) into PF side chains without the alkyl spacer **14** was carried out by Müllen and coworkers [26] to enhance blue PLED performance.

Here, TPA acts as soluble group and prevents the formation of aggregates and, in addition, can lower the hole-injection barrier between PF and ITO anode due to the closer Ip of TPA (5.3 eV) to the work function of the ITO anode (5 eV). However, for the device configuration (ITO/PEDOT:PSS/**14**/Ba), this TPA-containing PF, **14**, did not improve device performance as compared to PFO or **3**. This was attributed to the lower PLQE of **14** film (22%) than that of PFO film (50%) and the hole-trap property of TPA. In addition, its EL spectrum exhibited a pale blue emission (main peak at 428 nm) with CIE coordinates of (0.184, 0.159).

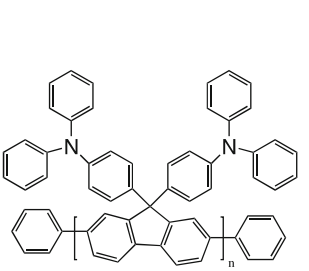

14

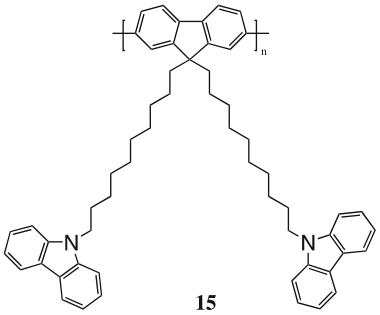

15

Our group has incorporated the HTM carbazole (Cz) into PF side chains by connecting this group with flexible decyl spacers. The device based on the polymer **15** with the configuration ITO/PEDOT:PSS/**15**/Ca/Al exhibits a turn-on voltage of 3.3 V, maximum efficiency of 1.28 cd A^{-1}, and maximum brightness of 5079 cd m^{-2}. The device emits sky blue light with two characteristic peaks at 420 and 460 nm, as for PFO, and an additional strong broad peak at 525 nm [27]. After further investigation [28], we found that the Cz groups in **15** play multiple roles as:

1. Hole transporters at the polymer–PEDOT:PSS interface to provide easier hole injection
2. Hole trapping sites (in the form of Cz/Cz dimers) able to catch electrons to form blue-emitting excitons
3. A source of green emission from an electroplex formed via electric field-mediated interaction of a Cz/Cz radical cation with an electron in the nearby PF backbone

On the other hand, Scherf and coworkers used *N*,*N*-bis(4-methylphenyl)-*N*-phenylamine as the end-capper to yield the polymer **16** (end-capper concentration 3 mol %); its single-layer device (ITO/PEDOT:PSS/16/Ca/Al) exhibited maximum luminance of 1600 cd m^{-2} and efficiency of 1.1 cd A^{-1}, with CIE coordinates (0.15, 0.08) at 8.5 V [29]. This efficiency is higher than that of non-end-capped polymer **3** (that is, bromine exists at each chain end) by one order of magnitude and was attributed to an efficient hole trapping at the

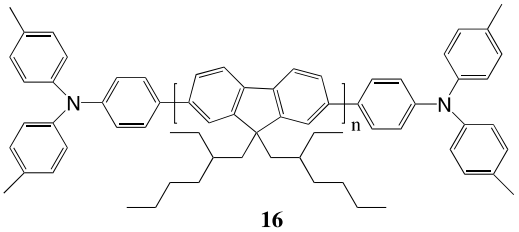

16

end-capper groups [due to the lower HOMO level of triarylamine (TAA) end-capper (5.48 eV) than **3** (5.88 eV)], resulting in more chances for holes and electrons to recombine on the main chain than at sites with less efficient emissions, such as aggregates and excimer-forming sites.

2.2.1.3 Incorporation of Electron-Transport Moiety (ETM)

For ETM incorporated in PF main chain, Jen and coworkers [30] presented copolymers with units of 9,9-dihexylfluorene and 2,5-dicyanobenzene and reported that the device based on the cyano (CN)-containing copolymer **17** as the emitting layer shows a low turn-on voltage (3 V) and better EL efficiency (0.5%) and high brightness (5430 cd m^{-2}) than those (0.044% and 717 cd m^{-2}) of the homopolymer **1** device with the same configuration (ITO/PEDOT:PSS/emitting polymer/Ca). The better device performance was attributed to the improved electron injection from the calcium cathode to the polymer because the CN electron-withdrawing functionality can lead to a significant increase of Ea from 2.12 eV of **1** to 2.98 eV of **17**, that is, close to the work function of the calcium cathode (2.9 eV). However, the EL spectrum of **17** is red-shifted (main emission peak at 477 nm) with respect to that of **1** (428 nm).

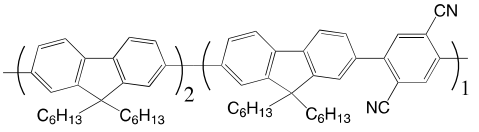

17

For PFs with HTM grafting as side chain, the alternating copolymer **18** with electron-deficient moiety (4-*tert*-butylphenyl-1,3,4-oxadiazole) functionalized fluorene and monomer of PFO was synthesized by Shu and coworkers [31]. The device with the configuration ITO/PEDOT:PSS/**18**/Ca/Ag showed improved performance: turn-on voltage of 5.3 V (defined as voltage needed for brightness of 1 cd m^{-2}), maximum brightness 2770 cd m^{-2} at 10.8 V, and maximum external quantum efficiency 0.52% at 537 cd m^{-2} rela-

tive to that of PFO (corresponding performance: 8 V, 600 cd m^{-2} at 20 V, and 0.2% at 17 V). This resulted from a better electron injection (LUMO 2.47 eV for **18** and 2.12 eV for PFO [12]; work function of Ca 2.9 eV) and transport in **18**. However, only little improvement was achieved, which could be due to the similar Ip between PFO (5.8 eV) and 4-*tert*-butylphenyl-1,3,4-oxadiazole (5.76 eV), leading to a significantly large hole-injection barrier from the anode (5.2 eV) to the emitting polymer. In addition, the EL spectrum of the device peaks at 428 nm and has no undesirable excimer/aggregate emission.

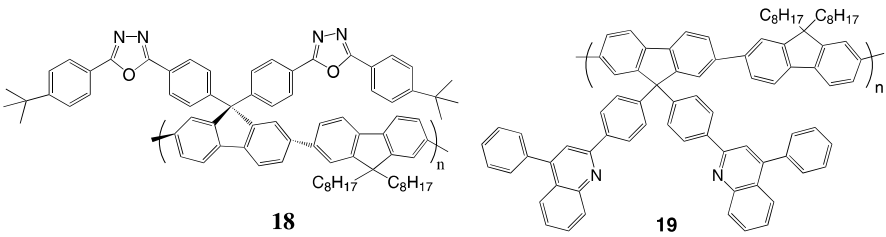

Another electron-deficient moiety, quinoline, was introduced into PF **19** by Su et al. [32]. However, the EL device performance (with the structure ITO/PEDOT:PSS/**19**/1,3,5-tris-(*N*-phenylbenzimidazol-2-yl)benzene (TPBI)/Mg:Ag) remains low, with the maximum external quantum efficiency of 0.8%, maximum luminance of 1121 cd m^{-2} and high turn-on voltage of 7.2 V. Therefore, the introduction of electron-deficient moieties (either 4-*tert*-butylphenyl-1,3,4-oxadiazole or quinoline) cannot provide efficient EL performance, probably due to the large hole-injection barrier.

Our group reported that capping both ends of the PFO chain with electron-deficient moieties (oxidazole, OXD, and triazole, TAZ), which can induce a minor amount of long conjugating length species (regarded as the β-phase),

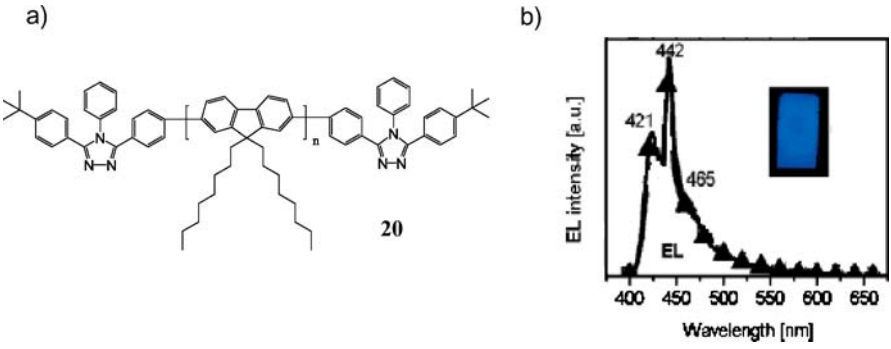

Fig. 3 **a** Chemical structure of polymer **20**. **b** EL spectra of spin-cast films of **20**. The *inset* shows picture of emission from **20**-based device operated at 4 V (taken from [33])

allowed an occurrence of incomplete energy transfer from the amorphous matrix to the β-phase and consequently resulted in a stable pure blue emission upon cyclic operations and promoted device efficiency [33]. For the case with TAZ (ITO/PEDOT:PSS/20/CsF/Al), the EL spectrum (in Fig. 3b) has a peak at 421 nm from the amorphous matrix and one at 442 nm from the β-phase, and gives the CIE coordinates (0.165, 0.076). Its maximum luminance efficiency (1.67 cd A^{-1}) and brightness (4000 cd m^{-2}) are better than those with *tert*-butylphenyl as end-capper, (0.74 cd A^{-1} and 2500 cd m^{-2}, respectively).

2.2.1.4 PFs with both HTM and ETM

In addition to the incorporation of a single charge-transport moiety on PFs, as mentioned above, simultaneously grafting electron-rich TAA and electron-deficient OXD groups on PF side chains was reported by Shu and coworkers [34]. This side-chain modification can lead to variations in both HOMO and LUMO levels. This polymer, **21**, showed maximum external quantum efficiency of 1.21% and luminance of 4080 cd m^{-2} at the device structure ITO/PEDOT:PSS/**21**/Ca/Ag. The enhanced efficiency was about twice that of the device with **18** as the emitting layer. This resulted from the better charge injection for **21** since its HOMO and LUMO levels (5.3 and 2.54 eV, respectively) are closer to the work functions of the ITO/PEDOT:PSS anode (~5.2 eV) and Ca cathode (2.9 eV) than **18** (HOMO 5.76 eV, LUMO 2.47 eV) and more efficient charge recombination (however, no evidence was given to support this claim).

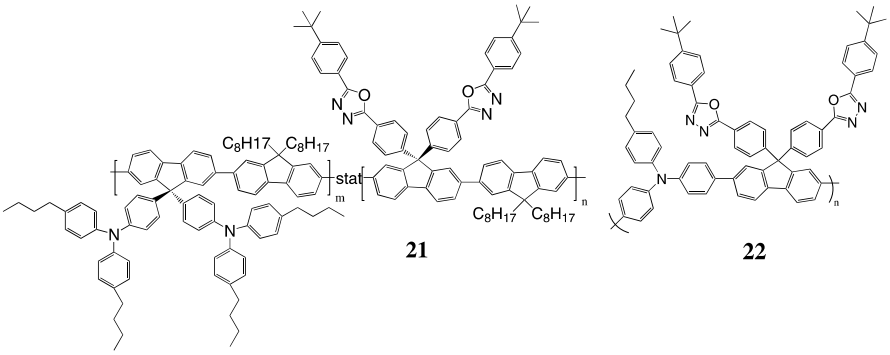

On the other hand, Shu and coworkers reported that the incorporation of TAA and OXD in PF main chain and side chains, respectively, provided an improvement in the efficiency and purity of blue emission (based on the device ITO/PEDOT/**22**/TPBI/Mg:Ag) to 2.07 cd A^{-1} and a CIE value of

$x + y = 0.29$, respectively, relative to those of **21** (corresponding performance: 1.66 cd A^{-1} and CIE $x + y = 0.3$) [35]. The HOMO and LUMO energy levels of **22** are 5.20 and 2.38 eV, respectively. No doubt the hole-injection ability of **22** can be improved as compared to that of **21** (HOMO 5.3 eV) because the *lower* HOMO energy level of **22** is better matched to the work function of the ITO/PEDOT:PSS electrode (5.2 eV) than that of **21**. But, the lower LUMO level of **22** (2.38 eV) than that of **21** (2.54 eV) cannot improve the electron-injection ability because the LUMO level of TPBI is 2.7 eV [36]. Therefore, we think that the reasons for the enhanced performance of the **22**-based device are still not clear and are in need of further investigation.

Another example of bipolar PF, **23**, was also reported by Shu and coworkers [37]. They claimed that the bulky hole-transport Cz-derivative provides more effective hole injection than **18**. The blue EL device, ITO/PEDOT:PSS/**23**/TPBI/Mg:Ag, exhibits a maximum external quantum efficiency of 1.0%, maximum luminance of 1070 cd m^{-2}, and turn-on voltage of 4.5 V.

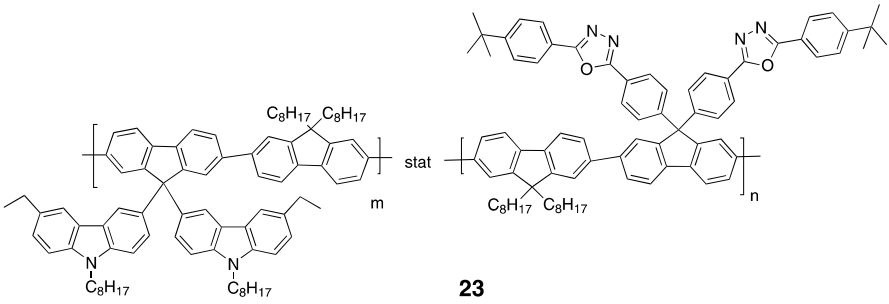

23

Shu and coworkers synthesized another kind of PF, **24**, with hindered dipolar pendent groups, TAA linked with OXD via a conjugated bridge, which was claimed to provide efficient charge transport/injection properties [38]. The

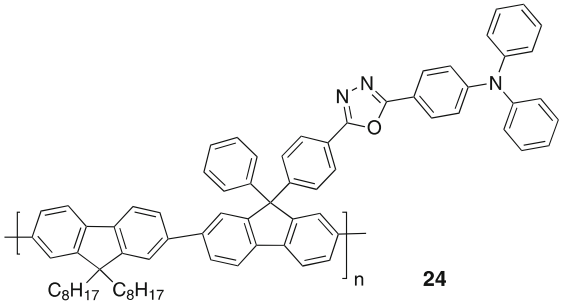

24

resulting EL device with the structure ITO/PEDOT:PSS/**24**/TPBI/Mg:Ag provides a maximum external quantum efficiency of 1.4%, maximum luminance of 2080 cd m^{-2}, and turn-on voltage of 5 V.

2.2.2 Physical Manipulation

Physical methods include tuning of chain conformation [39–42] and manipulation of supermolecular structure [43]. Because of its highly coplanar backbone, PFO can be physically transformed into a variety of supermolecular structures [39–42], such as crystalline phases (i.e., α and α' phases) and non-crystalline phases (i.e., amorphous, nematic, and β-phase; for β-phases it has an extended conjugation length of about 30 repeat units as calculated from wide-angle X-ray diffraction measurements) [44]. However, studies on the effects of tuning chain conformation on EL are scarce, but reports on effects of manipulating supermolecular structures on PL behaviors of PFO are extensive [40–42, 44].

As mentioned in Sect. 2.2.1.3 [33], we proposed that a trace amount of β-phase, induced by the use of an electron-deficient moiety (TAZ) as an end-capper for PFO, can improve device performance to give a better blue purity. Following the idea of β-phase formation, we further proposed a novel simple physical method to generate β-phase at a content of up to 1.32% in a PFO film spin-coated on a substrate (the remaining part is amorphous phase) by immersing it in a mixed solvent/non-solvent (tetrahydrofuran/methanol) for a few seconds [45]. The device based on PFO with 1.32% β-phase (ITO/PEDOT:PSS/emitting polymer/CsF/Al) has a dramatically enhanced device efficiency and an improved blue-color purity of 3.85 cd A^{-1} (external quantum efficiency, 3.33%) and CIE of $x + y = 0.283$ (less than the limit of

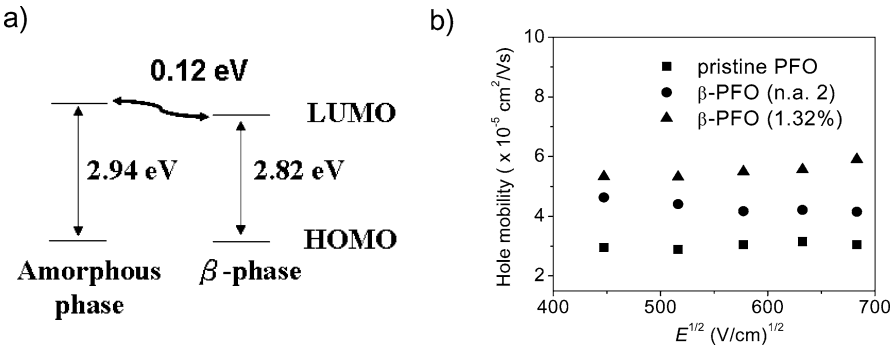

Fig. 4 **a** Energy-level diagram for the amorphous and β-phases. **b** Electric-field (E)-dependent hole mobilities of pristine PFO (as spin-coated without dipping), β-PFO (n.a. 2) (*n.a. 2* denotes trace β-phase content), and β-PFO (1.32%) (taken from [45])

0.3 for pure blue), relative to that without such treatment, 1.26 cd A^{-1} (1.08%) and $x + y = 0.323$. Such a high efficiency (the highest among the reported pure-blue-emitting devices) results from the special functionalities of the β-phase: electron-trapping (see Fig. 4a) and promoted hole mobility (see Fig. 4b as revealed from thin-film TOF measurements). The energy levels in Fig. 4a were determined from UV absorption spectra and CV and are supported by thermally stimulated current (TSC) data. Because holes are minor charge carriers in pristine PFO, these two characteristics will lead to more balanced hole and electron fluxes and thus higher device performance. In addition to the improved purity of blue emission, the β-phase can also enhance the stability of blue emission during cyclic operation because: (1) linear alkyl side chains of the β-phase chains located beside fluorene units [46] can hinder neighboring PFO main chains from the intimate contact needed to form green-emitting field-induced excimers [47], and (2) efficient Förster energy transfer from the amorphous to the β-phase can also prevent formation of excimers.

2.3
Sources of Undesirable Green Emission in PF-based PLEDs

An important issue concerning whether PFs can act as pure-blue emitters is undesirable green emission (480–650 nm), and investigations on such additional lower energy emission have been intensive recently. Early reports attribute it to the aggregate/excimer emissions due to the stiff and planar chain geometry of the PF backbone [48]. As reported by Weinfurtner et al. [49], oligomers with molecular weight of less than 10 000 Da can give this green emission (main peak at 510 nm) due to the ease of aggregate formation. In addition, polar end group-enhanced aggregation emission at 507 nm for PFO without end-capping (the end groups are boron ester on one end and bromine groups on the other end) was demonstrated by us to be another reason for green emission [50]. However, several research groups directly attributed this phenomenon to the chemical defects on the PF main chain (i.e., keto defect or fluorenone) that emit green light at 535 nm [51–55]. Recently, we found that electric field induction (FI) accompanied by side-chain motion in PFs can lead to formation of excimers, which contribute to a growth of the green component peaking at 485 and 520 nm in the EL spectrum [47]. We also revealed that higher polarity of the side chain in PFs can cause a more pronounced FI effect. For polymer **25** having cross-linkable highly polar oxtane groups at the ends of the side chains, the green component can even dominate the entire emission after a few cycles of device operation. Lowering the content of the cross-linkable commoner in the copolymers with DOF from 50 to 25 mol %, or even cross-linking **25**, only moderately suppresses the formation of FI excimers. This phenomenon also occurs for PFO with non-polar octyl side chains, especially after cyclic operations with higher electric fields

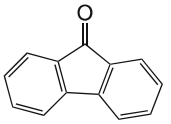

Fluorenone

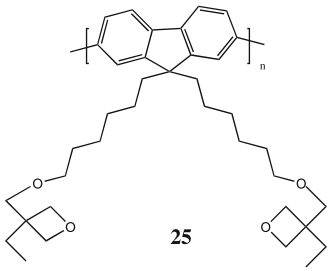

25

(1×10^6 V cm^{-1}). Thus, we must emphasize that there are several sources of the undesired green emission.

3
PFs with Various Emission Colors

3.1
Green and Red Emitters

Because the red-, green-, and blue-emitting polymers are essential in the fabrication of full-color PLED displays, fluorene copolymers that emit colors covering the entire visible range have been extensively studied and their syntheses are mainly via the Suzuki or Yamamoto routes [56]. However, more efforts have been made on the development of green- and red-emitting PF copolymers because PF homopolymer itself emits blue light. In this section, we review typical cases based on chemical incorporation of a fluorescent or phosphorescent moiety on PF for color tuning.

3.1.1
Chemical Strategy via Fluorescent Moiety Incorporated in Polymer Backbone, Side Chain, or Chain End

Heeger and coworkers adopted bithiophene as comonomer to copolymerize with fluorene and found that the EL emission can be tuned to emit green light with a peak at 493 nm and a shoulder at 515 nm [57]. The HOMO and LUMO energy levels of copolymer **26** are 5.30 and 2.85 eV, respectively, as estimated

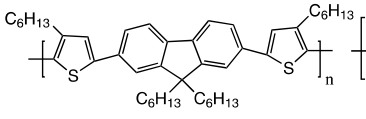

26

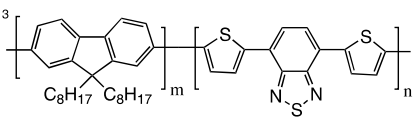

27: m = 85, n = 15

from the oxidation and reduction onset potentials of CV measurements. The single layer device (ITO/**26**/Ca) emitted green light at about 21 V. By employing a PVK layer (90 nm) between the ITO anode and the emitting polymer film as hole-injection layer, the turn-on voltage for light output of the double-layer device was reduced to about 8 V, and the maximum external quantum efficiency increased from 0.05 to 0.6%.

After that, Cao and coworkers synthesized a series of copolymers derived from DOF and narrow-band-gap 4,7-di-2-thienyl-2,1,3-benzothiadiazole (DBT) with various feed ratios of DOF/DBT [58]. The highest quantum efficiency and brightness were only 1.4% and 259 cd m^{-2}, respectively, from the device based on the copolymer with 15% DBT content (ITO/PEDOT:PSS/**27**/Ba/Al). As DBT content increases from 1 to 35%, the EL emission peak shifts from 628 nm to 674 nm, indicating that the copolymers are promising candidates as pure-red emitters though the performance needs to be further improved.

Another PF copolymer **28**, composed of alternating DOF and thieno-[3,2-*b*]thiophene, was reported by Lim et al. [59]. The incorporation of electron-rich thieno-[3,2-*b*]thiophene moiety in the polymer backbone led to lower HOMO (5.38 eV) and higher LUMO (2.4 eV) levels than those of PFO (HOMO 5.8 eV, LUMO 2.12 eV [12]). The device ITO/PEDOT:PSS/**28**/LiF/Al exhibited a pure green emission with a peak at 515 nm and CIE coordinates of (0.29, 0.63), which is very close to the standard green required by the National Television System Committee (NTSC) (0.26, 0.65). In addition, the maximum brightness and efficiency of this device were 970 cd m^{-2} and 0.32 cd A^{-1}, respectively.

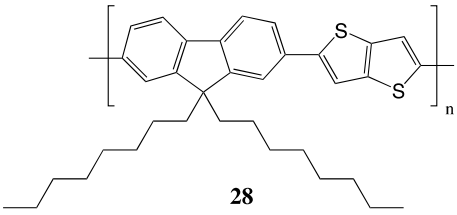

28

Jen and coworkers reported random copolymers with 5 and 10 mol % of electron-deficient dithienosilole chromophore (**29** and **30**, respectively) [60]. The device with **30** as the emitting layer and an in-situ polymerized bis-tetraphenylenebiphenyldiamine-perfluorocyclobutane, **31**, as the HTL (ITO/**31**/**30**/Ca) can emit green light (λ_{max} = 500 nm) with the low turn-on voltage of 4 V, maximum brightness of 25 900 cd m^{-2}, and maximum external quantum efficiency of 1.64%, which are much better than the device with **29** as the emitter. This improvement was attributed to both an improved charge injection and to charge recombination in this higher dithienosilole-containing copolymer **30** because its HOMO and LUMO levels (5.5 and

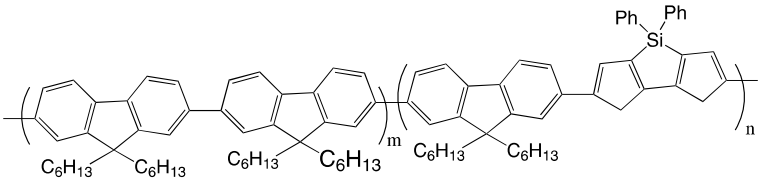

29: **m = 19, n = 1**
30: **m = 9, n = 1**

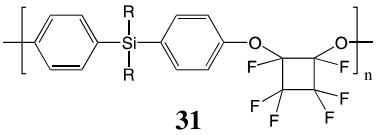

31

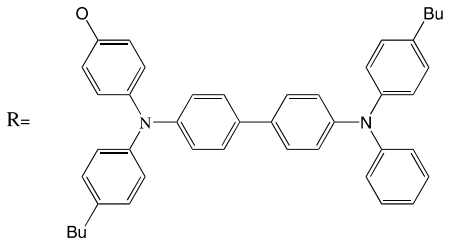

2.32 eV, respectively) are closer to the HOMO level of **31** (5.32 eV) and work function of Ca (2.9 eV) than those of **29** (5.68, and 2.18 eV, respectively).

Müllen and coworkers [61] incorporated perylene dyes to PF chains as:

1. Comonomers in the main chain
2. End-capper at the chain ends
3. Pendant side groups to tune emission color covering the whole visible range

For case (1), copolymers with various chemical structures of perylene can exhibit green and red light. For example, based on ITO/PEDOT:PSS/emitting polymer/Ca/Al, EL emission from **32** showed green light with a peak at 520 nm [CIE coordinates (0.362, 0.555)], and the emission from **33** was deep red [CIE coordinates (0.636, 0.338)] with a maximum at 675 nm. The maximum EL efficiencies for the PLEDs using **32** and **33** were 0.9 and 1.6 cd A^{-1}, respectively. For case (2), polymer **34** exhibited a narrow red photoluminescence (PL) emission with a maximum at 613 nm in the film state via an almost complete energy-transfer mechanism from fluorene units to perylene end-cappers, but the energy transfer was not seen in solution. For case (3), copolymer **35** containing 33 mol % of fluorene units with pendant dyes as a film exhibited a PL emission maximum at 599 nm. Even in solu-

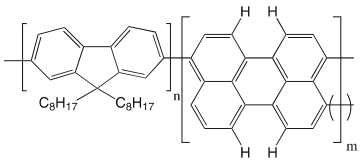

32

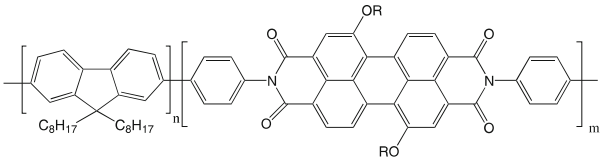

33

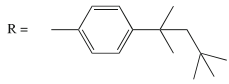

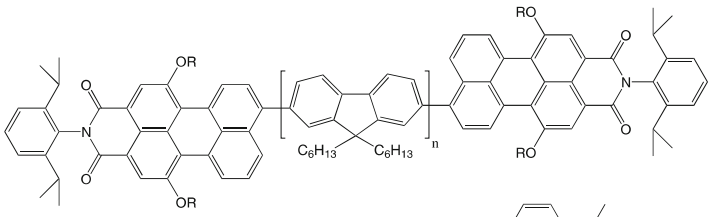

34

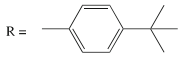

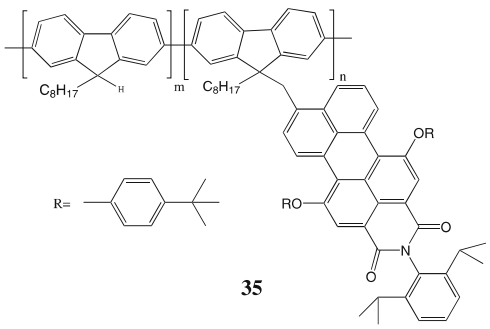

35

tion, efficient energy transfer to the pendant groups was clearly apparent, as evidenced by the PL emission of a peak at 561 nm and a shoulder at 599 nm, due to the higher concentration of perylene units in the polymer than case (2).

Cho et al. prepared **36** by incorporating low-band-gap thiophene together with CN-substituted vinylene, which gives pure red EL emission [CIE coordinates (0.66, 0.33)] that is almost identical to the standard red (0.66, 0.34) demanded by the NTSC [62]. Another similar copolymer **37** also exhibited a pure red emission [CIE coordinates (0.63, 0.38)], and its maximum

luminance and maximum external quantum efficiency were approximately 3100 cd m^{-2} at 4.6 V, and 0.46% at 4 V, respectively, which are better than those of **36**. The difference between **36** and **37** is the position of CN groups on the vinylene unit. The CN group in the latter was at β-position, and this configuration caused a strong steric interaction of CN groups with the alkoxy side chains of the inner phenylene ring, which shortens the conjugation length of the molecules and therefore results in a blue-shift in the emission (630 nm) relative to the former (675 nm).

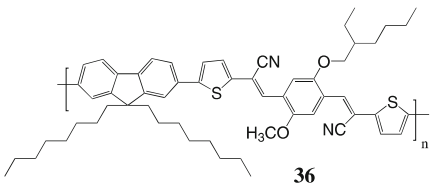

36

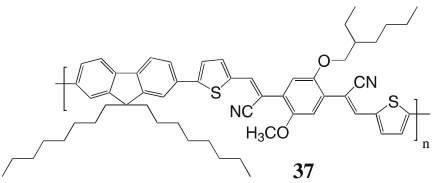

37

Dow Chemical Company presented a series of PF copolymers, consisting of various charge-transport moieties and low band-gap chromophores on the backbone, for tuning the emission color of PLED to cover the whole visible range [63]. They claimed that their blue-, green-, and red-emitting copolymers (without disclosing chemical structures and ratios of comonomers) can exhibit acceptable device performance, as shown in Table 1.

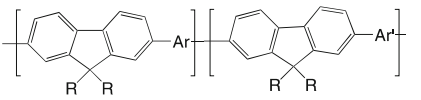

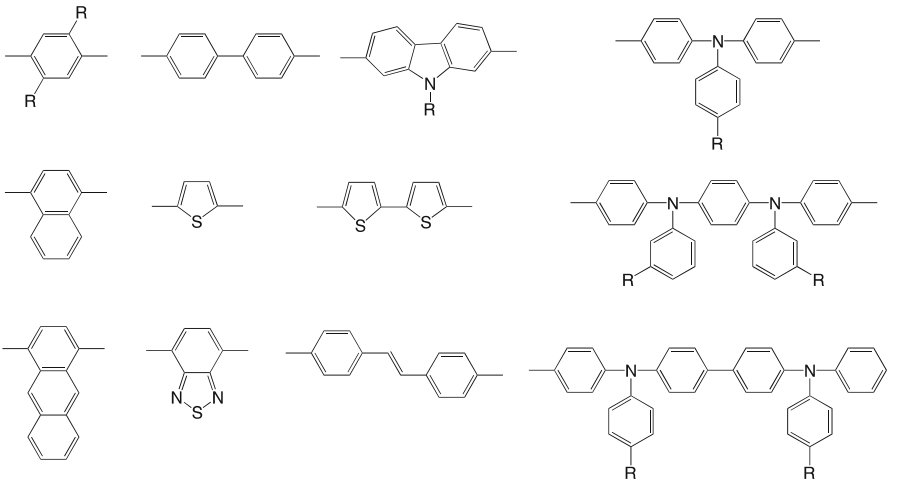

Table 1 Characteristics of device performance based on ITO/PEDOT:PSS/copolymer/Ca/Al configuration (taken from [63])

	Green	Red	Blue
EL λ_{max} [nm]	534	648	476
CIE (x, y) [a]	(0.40, 0.58)	(0.68, 0.32)	(0.16, 0.16)
Efficiency [lm W^{-1}, cd A^{-1}]			
200 cd m^{-2}	7.64, 6.92	1.43, 1.50	1.31, 2.82
1000 cd m^{-2}	8.31, 8.84	0.68, 1.2	0.90, 2.60
4000 cd m^{-2}	7.36, 10.01	–, –	0.48, 2.00
10 000 cd m^{-2}	5.62, 10.25	–, –	–, –

[a] Measured at 200 cd m^{-2}

3.1.2 Chemical Strategy via Phosphorescent Moiety Incorporated in Polymer Side Chain and Backbone

In addition to the incorporation of fluorescent chromophores in PF, phosphorescent moieties have been widely used to copolymerize with fluorene or as pendent group in PFs for color tuning (via the selection of ligands chelated to heavy metals) and performance improvement. The ability to enhance device performance via phosphors is because strong spin–orbit coupling (resulting from the inclusion of heavy metal atoms in the phosphor structure) can efficiently utilize triplet excitons for electroluminescence and theoretically there are three times as many as triplet as singlet excitons.

Our group reported a new route for the design of electroluminescent polymers by grafting high-efficiency phosphorescent iridium complexes as dopants and charge-transport moieties onto alky side chains of fully conjugated polymers for PLED with single layer/single polymers [27]. As shown in Fig. 5a, the polymer system studied involves PF as the base-conjugated polymer, Cz as the charge-transport moiety and a source for green emission by forming an electroplex with the PF main chain (as revealed above), and cyclometalated Ir complexes as phosphorescent dopants. The devices prepared therewith (ITO/PEDOT:PSS/**38** or **39**/Ca/Al) can emit red light with the high efficiency of 2.8 cd A^{-1} at 7 V and 65 cd m^{-2} from **38** (with high Ir complex content of 1.3 mol % in the feed), and can emit the light with a broad band containing blue, green, and red peaks (2.16 cd A^{-1} at 9 V) from **39** (with low Ir complex content of 0.8 mol % in the feed) as shown in Fig. 5b. The inset of Fig. 5b shows that the HOMO and LUMO (the triplet state) energy levels of the red Ir complex lay between those of the main chain, which permits both hole and electron trapping during the electric field excitation.

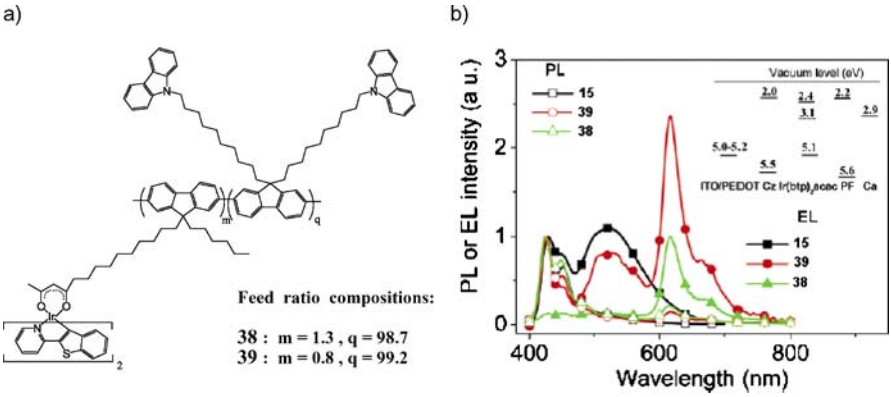

Fig. 5 **a** Chemical structures of Ir-complex and Cz-moiety grafted PFs. **b** PL and EL spectra of the polymers. Also shown is the band diagram, in which the LUMO for $Ir(btp)_2acac$ has the energy level for singlet state at 2.4 and triplet state at 3.1 eV (taken from [27])

Holmes and coworkers [64] reported a series of solution-processible phosphorescent iridium complexes with iridium units being covalently attached to and in conjugation with oligo(9,9-dioctylfluorenyl-2,7-diyl) $[(FO)_n]$ to form complexes $[Ir(ppy\text{-}(FO)_n)_2(acac)]$ or $[Ir(btp\text{-}(FO)_n)_2(acac)]$. Based on ITO/PEDOT:PSS/emitting polymer/Ca/Al, $[Ir(ppy\text{-}(FO)_n)_2(acac)]$ with $n = 10$ (**40**) and 30 (**41**) emitted mostly triplet emission at 570 and 612 nm but with a small peak (444 nm) due to PF singlet emission. $[Ir(btp\text{-}(FO)_n)_2(acac)]$ with $n = 5$ (**42**), 10 (**43**), 20 (**44**), and 40 (**45**) all showed exclusive triplet emissions in their EL spectra (main peaks around 665 nm) pointing to charge trapping at the iridium complex being the dominant process under EL excitation. EL efficiencies are larger for $[Ir(ppy\text{-}(FO)_n)_2(acac)]$ with longer FO segments (0.045% for **40** and 0.07% for **41**), and this increasing trend of EL efficiencies with longer FO segments also occurs for $[Ir(btp\text{-}(FO)_n)_2(acac)]$ (0.15, 0.2, 0.45, and 1.5% for **42**–**45**, respectively). These results might be due to the reduced self-quenching for polymer with longer FO segments (namely, lower concentration of Ir complex).

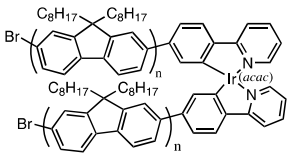

40: n = 10, 41: n = 30

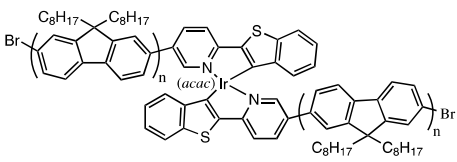

42: n = 5, 43: n = 10, 44: n = 20, 45: n = 40

Cao and coworkers synthesized copolymers **46** (feed ratio of Ir complex is 3 mol %) with 9,9-dihexylfluorene-*alt*-*N*-2-ethylhexyl-carbazole segments and backbone β-diketonate moieties coordinating to iridium [65]. A satu-

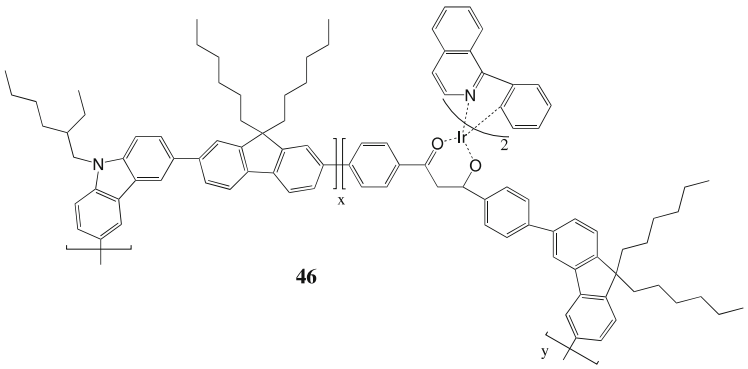

46

rated red-emitting PLED with the emission peak at 628 nm, maximum external quantum efficiency of 0.6% at 38.5 mA cm^{-2}, and maximum luminance of 541 cd m^{-2} at 15 V were achieved from the device ITO/PEDOT:PSS/**46** blended with 2-(4-biphenylyl)-5-(4-*tert*butylphenyl)-1,3,4-oxadiazole (40%)/Ba/Al. For **46**, the incorporation of Cz and iridium complex units in the backbone can reduce its barriers for both hole and electron injections, as compared with PFO, because its HOMO and LUMO levels (5.49 and 2.47 eV, respectively) are closer to the work functions of PEDO:PSST (4.9 eV) and Ba (2.2 eV) than those of PFO (5.77 and 2.91 eV, respectively).

3.2 White Emitters

In addition to green- and red-light emitters, white PLEDs have also received great attention due to their potential applications in backlight for full-color displays and lighting.

3.2.1 Physical Blending System

Due to the many reported examples utilizing physical blending systems, we have only selected a few important examples for this section. Shu and coworkers used the blend of the blue-emitting PF, **21**, with two fluorene-derived fluorescent dyes [66], FFBFF (green emitter) and FTBTF (red emitter), to realize white light emission. The resulting EL device (ITO/PEDOT:PSS/**21** with 0.18 wt. % FFBFF and 0.11 wt. % FTBTF/Ca/Ag) exhibited maximum external quantum efficiency of 0.82% and maximum luminance of 12 900 cd m^{-2}; while its EL spectra changed with the applied voltages (from CIE coordinates (0.36, 0.37) at 6 V to (0.34, 0.34) at 12 V).

We prepared two PFs, **47** and **48**, which exhibited rather high bipolar charge mobilities in the order of 10^{-3} to 10^{-4} cm^2 V^{-1} s^{-1} [67]. The light-

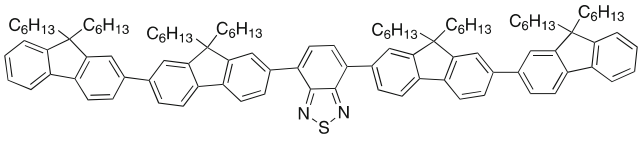

FFBFF

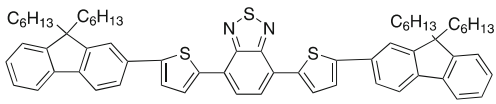

FTBTF

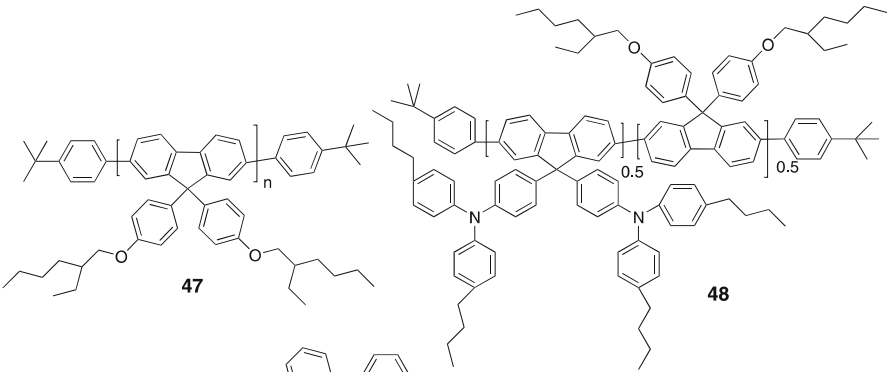

47 48

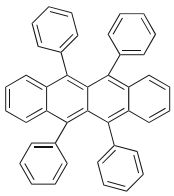

Rubrene

emitting devices (ITO/PEDOT:PSS/emitting layer/CsF/Ca/Al) with rubrene-doped **47** showed the maximal luminances 36 000 and 70 000 cd m^{-2} with the maximal efficiencies 3.5 and 9 cd A^{-1} for the white (doped with 0.25 wt. % rubrene) and yellow emissions (doped with 0.5 wt. % rubrene), respectively. For rubrene doped **48**, the maximal luminance and efficiency are 56 000 cd m^{-2} and 9 cd A^{-1} for white-emitting devices, and 72 000 cd m^{-2} and 14 cd A^{-1} for yellow emission, respectively. Furthermore, the EL profiles of the investigated devices are nearly independent of the applied voltages.

3.2.2
Chemical Strategy: Single-Polymer Approach

To yield white emission, it is difficult to generate emissions covering the whole visible region via a single polymer. Moreover, blending systems (poly-

mer/polymer or polymer/molecular material) to realize white-light emission usually suffer from intrinsic phase separation and bias-dependent spectra. Therefore, creation of a strategy to realize white light from a single polymer is necessary.

The first example of a white PLED achieved by a single polymer with SPF backbone was realized by Covion Corporation [68]. The white-light emitting polymers (the detailed chemical structures were not disclosed) were synthesized by copolymerization of PPV monomer unit (emits green) and bisthiophenylbenzothiadiazole (emits red) derivatives onto the SPF backbone. The device (ITO/PEDOT:PSS/polymer/Ba/Al) emitted white light with CIE coordinates (0.36, 0.41) and exhibited a maximum efficiency of 7.8 cd A^{-1} and a maximum luminance of ca. 10 000 cd m^{-2}.

Shu and coworkers developed white-light emitting polymers **49** through incorporating benzothiadiazole (emits green) and bisthiophenylbenzothiadiazole (emits red) moieties into the backbone of a blue bipolar PF [69]. White electroluminescence can be achieved via incomplete energy transfer. The white [CIE coordinates (0.37, 0.36)] EL device based on this PF (ITO/PEDOT:PSS/ **49**/TPBI/Mg:Ag/Ag) exhibits a maximum external quantum efficiency of 2.22%, maximum luminance of 5000 cd m^{-2}, and high turn-on voltage of 5.5 V.

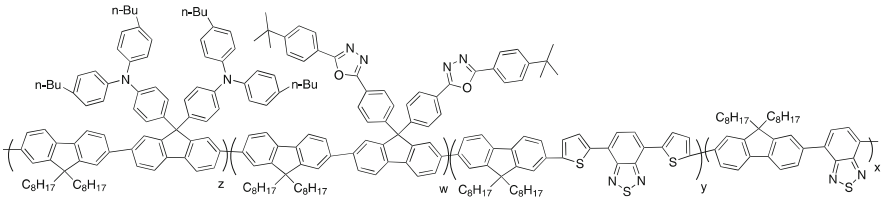

49

Another example using the same methodology was achieved by Shu and coworkers [70], the white light-emitting polymer **50** is realized by covalently

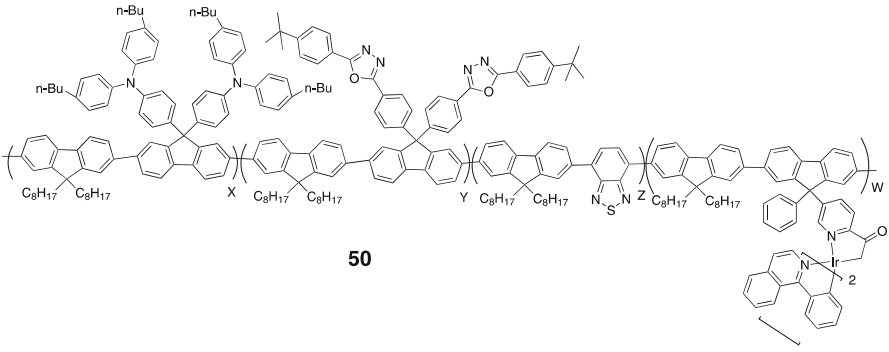

50

attaching a green fluorophore as well as a red phosphor into the backbone of bipolar PF. The EL device (ITO/PEDOT:PSS/**50**/CsF/Al) exhibited a maximum efficiency of 8.2 cd A^{-1}, maximum luminance of ca. 4000 cd m^{-2}, and low turn-on voltage of 2 V, but with drifted white emissions from CIE coordinates (0.35, 0.38) to (0.33, 0.36).

4
Alteration of Interfaces Between PFs and Electrodes

In order to achieve better hole or electron injection for enhancement of device performance, introduction of appropriate hole-transport and electron-injection materials into the interfaces of anode/PFs and PFs/cathode, respectively, is another useful approach in addition to the chemical and physical modifications of PF chain structure. Besides, choosing a cathode material with a work function close to LUMO levels of PFs has been proven to be a practical method for performance improvement.

4.1
Hole-Transporting Layer

He et al. reported a high-performance electroluminescence device based on bilayer conjugated polymer structures consisting of a hole-transport polymer **51** and a green-emissive polymer **52** prepared by the spin-coating technique on a glass substrate [71]. With this insertion of hole-transporting polymer, the device showed a high brightness (~10 000 cd m^{-2} at 0.84 mA mm^{-2}), good emission efficiency (~14.5 cd A^{-1}) and luminous efficiency (2.26 lm W^{-1}), and high external quantum efficiency (3.8%).

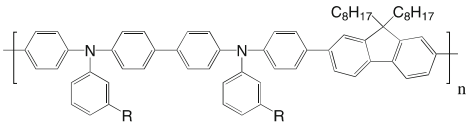

51

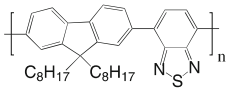

52

Marks and coworkers used a siloxane-derived hole-transport material, 4,4′-bis[(*p*-trichlorosilylpropylphenyl)phenylamino]biphenyl (TPD-Si_2), to modify the ITO anode surface via formation of a self-assembly monolayer (SAM) [72]. Due to the close Ip of TPD-Si_2 (5.5 eV) to the HOMO level of PFO (5.9 eV), the PFO-based device with ITO anode treated with TPD-Si_2 SAM exhibited a maximum brightness and external quantum efficiency of 7000 cd m^{-2} and 0.35%, respectively, which were about two orders of magnitude larger than those for the bare ITO device (work function of ITO 4.7 eV).

Even compared to a device with PEDOT:PSS (HOMO 5.2 eV) as HTL, the SAM-modified device exhibited higher maximum brightness by a factor of three, and a comparable efficiency.

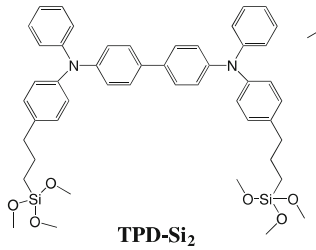

TPD-Si$_2$

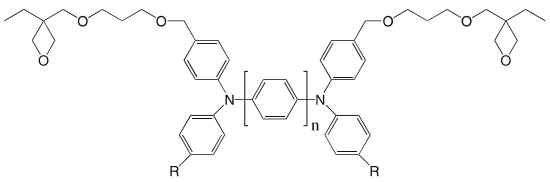

HTA 7: n = 1, R = H
HTA 8: n = 2, R = OMe
HTA 9: n = 2, R = H

In order to achieve a better hole injection via the concept of graded HTL, Müller et al. synthesized a series of cross-linkable oxetane-functionalized hole-transporting TAA (HTA 7, 8, 9) with different HOMO levels (5.29, 5.41, and 5.48 eV, respectively) [73]. They reported that the device based on graded HTL (spin-coating and then cross-linking in the order HTA 7, 8, and 9) and polymer **16** (end-capper feed ratio 0.3%) exhibited a better efficiency of 2.7 cd A^{-1} than the 0.64 cd A^{-1} of the device with only HTA 9, demonstrating that the graded HTL concept is useful in improving hole-injection ability.

Further, Friend and coworkers [74] demonstrated molecular-scale interface engineering, also based on the graded HTL concept, for an improvement of hole injection from ITO anode to emitting layer consisting of PFO blended with 5 wt. % **52**. The PEDOT:PSS materials with different doping levels from saturated–doped (charge-per-ring ratio $y = 0.3$, designated as p^{++}), to the intermediate doping levels of $y = 0.25$ and 0.2 (designated as p^{+} and p, respectively), and to the lowest doping level of $y = 0.02$ (designated as i) can be acquired via reducing as-received PEDOT:PSS (saturated–doped) by various equivalent moles of hydrazine hydrate. The device with the graded (PEDOT:PSS/**53**)$_5$(PSS/**53**) ($2p^{++}$-p^{+}-p-i) interlayer between ITO and emitting layer exhibited a current density more than twice as large as the p^{++}-PEDOT:PSS device, and four times that of the i-PEDOT:PSS device (here, calcium was used as cathode for all devices). This result further demonstrates that appropriate grade HTL can improve hole injection into the emitting layer.

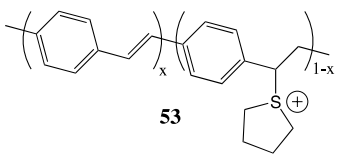

53

Although PEDOT:PSS is one of the most often adopted hole-transport materials, fundamental knowledge about how the process parameters (such as film thickness, backing conditions after coating, etc.) of this material affect PLED behaviors is still inadequate. Our group has demonstrated that migration of PSS from PEDOT:PSS into emitting layer may exert significant effects on the effective hole-injection barrier in blue-light emitting devices based on PFO [75]. In comparison to the hole-injection barrier 0.9 eV for bare ITO, the introduction of a PEDOT:PSS layer actually decreases the hole-injection barrier because the hole-injection barrier from PEDOT:PSS to PFO increases from 0.5 to 0.85 eV while PEDOT:PSS film thickness increases from 10 to 50 nm. This result was attributed to *p* –doping of PFO at the interface by free PSS chains. The thinner PEDOT:PSS film provides less *p* –doping and thus a lower hole-injection barrier. Therefore, the PFO-based PLED (ITO/PEDOT:PSS/PFO/CsF/Ca/Al) with lower PEDOT:PSS thickness (15 nm) can exhibit the highest device brightness and efficiency (8374 cd m^{-2} and 0.75 cd A^{-1}, respectively) among those devices with thicker PEDOT:PSS films (3000 cd m^{-2} and 0.5 cd A^{-1} for 50 nm thick PEDOT:PSS).

In addition to the effect of PEDOT:PSS film thickness on the hole-injection barrier, our group [76] found that the Ip value of PEDOT:PSS spin-coated onto the ITO anode decreases as the delay time to baking after spin-coating increases, from 5.45 eV (0 h) to 5.32 eV (48 h) as shown in Fig. 6. The trend moves toward the Ip of the neutral PEDOT, around 3.93–4.0 eV [77, 78]. This results in an increase of the hole-injection barrier to emitting polymer (PFO). The IP change was attributed to dedoping of PEDOT in PEDOT:PSS due to a reaction of ITO with protons in PSS and with those in doped PEDOT in the presence of water. Based on the device configuration of ITO/PEDOT:PSS/PFO/CsF/Ca/Al with PEDOT:PSS film varying with delay time to baking, the maximum brightness and efficiency are 15 600 cd m^{-2} (9 V) and 3.3 cd A^{-1} (3 V), respectively, for the device without delay. These are better than those for the device with 6 h delay (corresponding

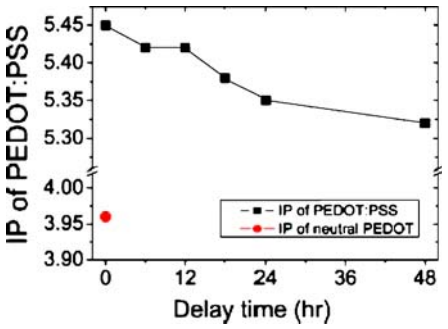

Fig. 6 IP values of 20 nm PEDOT:PSS films at different delay times to baking after spin-coating on ITO, and IP of neutral PEDOT (taken from [76])

Table 2 Ionization potential and the F/C atom ratio of the three CFx layers (taken from [79])

CFx layer	Ionization potential [eV]	F/C ratio
CFx (20 W)	5.7	1.51
CFx (35 W)	5.6	1.47
CFx (50 W)	5.3	1.33

performance: 1.9 cd A^{-1} at 3 V and 10 000 cd m^{-2} at 9 V). In other words, PEDOT:PSS film should be baked right after spin-coating in order to get better performance of the bipolar device.

Introduction of CFx thin film on top of the ITO anode as HTL via plasma polymerization of CHF_3 can also enhance device performance of PFO-based PLED, as reported by us [79]. At the optimal C/F atom ratio using the radio frequency power 35 W (see Table 2) as determined by X-ray photoelectron spectrometer, the device performance based on the ITO/CFx(35 W)/PFO/CsF/Ca/Al configuration is optimal having maximum current efficiency of 3.1 cd A^{-1} and maximum brightness of 8400 cd m^{-2}; much better than 1.3 cd A^{-1} and 1800 cd m^{-2} for the device with PEDOT:PSS as HTL. The improved device performance was attributed to a better balance between hole and electron fluxes because the CFx (35 W) layer possesses an Ip value of 5.6 eV (see Table 2), as determined by ultraviolet photoelectron spectroscopy data, and therefore causes a lower hole-injection barrier to the PFO layer (0.2 eV) than that of 0.7 eV for PEDOT:PSS.

4.2 Cathode Materials and Electron-Injection/Hole-Blocking Layer

The most straightforward approach to facilitate electron injection from cathode to emitting layer is to choose the cathode material with work function close to the LUMO level of the emitting layer for a reduction of the electron-injection barrier [56]. As shown in Table 3, metals with various work function values can be chosen as optimum cathode for efficient electron injection. However, a minimization of the electron-injection barrier is difficult to achieve since low work-function metals (such as Ca, Mg, Li, and Cs) are highly reactive and can easily interact with the organic layer onto which they are evaporated to quench excitons [80]. In addition, these metals are sensitive to oxygen and moisture in the environment, causing a quick degradation of these metals if lacking proper encapsulation.

Recently, alkali-metal fluoride/metal bilayer cathodes, especially for LiF and CsF, have shown substantial electron-injection ability [80–82]. Friend and coworkers demonstrated the minimization of the electron-injection barrier with the use of LiF as bilayer cathode (LiF/Ca) via electroabsorption

Table 3 Electronic properties of common electrode metals (taken from [56])

Element	Ionization potential [eV]	Preferred work function [eV]
Cs	3.89	2.14
K	4.34	2.30
Ba	5.21	2.70
Na	5.14	2.75
Ca	6.11	2.87
Li	5.39	2.90
Mg	7.65	3.66
In	5.79	4.12
Ag	7.58	4.26
Al	5.99	4.28
Nb	6.88	4.30
Cr	6.77	4.50
Cu	7.73	4.65
Si	8.15	4.85
Au	9.23	5.10

measurements [80]. They found that the electron-injection barrier for the LiF/Ca cathode is the lowest among all the cathode materials (including Al, LiF/Al, Ca, CsF/Al, and LiF/Ca). The result is that the PFO-based device with LiF/Ca cathode (ITO/PEDOT:PSS/PFO/LiF/Ca/Al) exhibits the largest current density ($45\,mA/cm^2$) and highest luminance ($1600\,cd\,m^{-2}$) at the driving voltage of 5 V. However, there is still no consensus over the mechanism behind the enhancement of electron injection for the use of this bilayer cathode and several interpretations have been proposed, as summarized by this group [80].

In addition to the appropriate choice of cathode material for better electron injection, the insertion of an electron-injection layer between cathode and emitting polymer has been reported. Yang and coworkers introduced the nanoscaled interfacial layer, calcium acetylacetonate [$Ca(acac)_2$], between the aluminum cathode and green-emitting PF blend (5BTF8, consisting of 5 wt. % **52** and 95 wt. % PFO), which led to improved device efficiency ($28\,cd\,A^{-1}$ at $2650\,cd\,m^{-2}$), higher than the device using calcium/aluminum as the cathode by a factor of three [83]. This result was attributed to the multiple functions of $Ca(acac)_2$:

1. It enhanced the injection of electrons due to electrons being the minor charge carriers in 5BTF8
2. It provided a buffer layer to prevent the quenching of luminescence from the aluminum electrode
3. It behaved as a hole-blocking layer for increasing hole–electron recombination probability

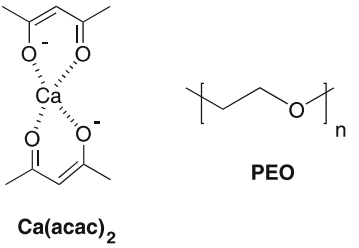

Another material, calcium carbonate (Cs_2CO_3), was applied to PFO-based PLED by Yang and coworkers and the luminous efficiency of a device with Cs_2CO_3/Al is higher than the device with only Ca as the cathode by a factor of 1.3, due to the better electron-injection and hole-blocking ability [84]. Recently, they also demonstrated that the improved electron injection is a result of the reaction of Cs_2CO_3 with thermally evaporated Al, which can reduce its work function to 2.1 eV by forming the Al–O–Cs complex. The optimum Cs_2CO_3 thickness is 15 Å with maximum power efficiency of 15 lm W^{-1} [85].

Recently, our group demonstrated a novel dual-functional composite layer having a superior hole-blocking effect along with promising electron-transport capability for PFO [86]. The dual-functional composite layer is composed of a non-conjugated polymer (polyethyleneoxide, PEO) as well as an inorganic salt (Cs_2CO_3), which allows an effective recombination of

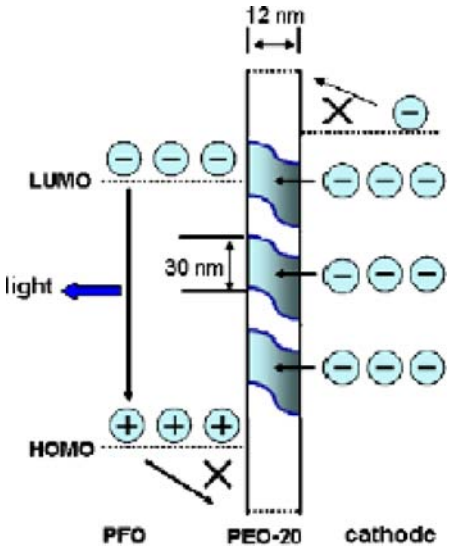

Fig. 7 Schematic diagram of charge-transport mechanism in PFO/PEO20/cathode. The *gray region* of the PEO20 layer is the Cs_2CO_3-rich region (taken from [86])

electrons and holes and results in a high device performance. In particular, a PFO-based device with this composite layer (PEO doped with 20 wt. % Cs_2CO_3, designated as PEO20) and a composite bilayer cathode Cs_2CO_3 (2 nm)/Ca (3 nm) (which can enhance the electron injection dramatically), ITO/PEDOT:PSS/PFO/PEO20/Cs_2CO_3/Ca/Al, gives a maximum brightness of 27 000 cd m^{-2} and current efficiency of 3.5 cd A^{-1} with pure blue emission at CIE coordinates (0.16, 0.07). This performance is better than that of the device without PEO20 [corresponding performance: 12 000 cd m^{-2}, 1.4 cd A^{-1}, and (0.16, 0.15)]. The hole-blocking effect of the composite layer is mainly because the incorporation of non-conjugated polymer PEO with high HOMO level can provide a large barrier for hole transport out of PFO (HOMO 5.8 eV). On the other hand, the presence of PEO film also reduces the electron current density (due to the large barrier for electron injection from cathode to PEO) but the addition of Cs_2CO_3 in PEO film can enhance the electron flux, indicating that the presence of Cs_2CO_3 in PEO acts as a channel for electron transport through the PEO film. The charge-transport mechanism in a PFO/PEO20/cathode is clearly illustrated in Fig. 7. In Fig. 7, electron carriers can smoothly transport through the PEO20 layer by passing through the Cs_2CO_3-rich region (electron-transport channel), but electron injection to the LUMO level of PEO is difficult. Furthermore, a majority of the hole carriers are blocked at the PFO/PEO20 interface and can effectively recombine with electron carriers.

5 Summary

The methods to improve performance of PF-based PLEDs in terms of emission efficiency, brightness, and operating voltage described in this review essentially promote a balance between hole and electron fluxes in the emitting layer and an enhancement of charge fluxes. The methods include modifying PF chain structures through chemical or physical methods, choosing a cathode material to minimize the electron-injection barrier, and inserting hole-transport and electron-injection layers to reduce hole- and electron-injection barriers, respectively. The chemical method, the incorporation of HTM or ETM into PF chains, can tune HOMO and LUMO levels of PFs to match the work functions of anode and cathode, respectively, and thus to enhance hole and electron fluxes. Physical manipulation on PF chain structures can achieve balanced hole and electron fluxes; for example, the presence of β-phase can provide electron trapping and promoted hole mobility and result in the highest device performance (3.85 cd A^{-1} and 34 300 cd m^{-2}) among the reported pure-blue PLEDs. Color tuning to cover all visible regions can be achieved via physical blending or chemical incorporation of PFs with fluorescent or phosphorescent chromophores.

References

1. Burroughes JH, Bradley DDC, Brown AR, Marks RN, Mackay K, Friend RH, Burns PL, Holmes AB (1990) Nature 347:539
2. Kraft A, Grimsdale AC, Holmes AB (1998) Angew Chem Int Edit 37:402
3. Horowitz G (1998) Adv Mater 10:365
4. Ling MM, Bao ZN (2004) Chem Mater 16:4824
5. Svensson M, Zhang FL, Veenstra SC, Verhees WJH, Hummelen JC, Kroon JM, Inganäs O, Andersson MR (2003) Adv Mater 15:988
6. Coakley KM, McGehee MD (2004) Chem Mater 16:4533
7. Ariu M, Lidzey DG, Lavrentiev M, Bradley DDC, Jandke M, Strohriegl P (2001) Synth Met 116:217
8. Bernius MT, Inbasekaran M, O'Brien J, Wu WS (2000) Adv Mater 12:1737
9. Neher D (2001) Macromol Rapid Commun 22:1365
10. Scherf U, List EJW (2002) Adv Mater 14:477
11. Baldo MA, O'Brien DF, You Y, Shoustikov A, Sibley S, Thompson ME, Forrest SR (1998) Nature 395:151
12. Janietz S, Bradley DDC, Grell M, Giebeler C, Inbasekaran M, Woo EP (1998) Appl Phys Lett 73:2453
13. Woudenbergh TV, Wildeman J, Blom PWM, Bastiaansen JJAM, Langeveld-Voss BMW (2004) Adv Funct Mater 14:677
14. Redecker M, Bradley DDC, Inbasekaran M, Woo EP (1998) Appl Phys Lett 73:1565
15. Redecker M, Bradley DDC, Inbasekaran M, Woo EP (1999) Appl Phys Lett 74:1400
16. Chua LL, Zaumseil J, Chang JF, Ou ECW, Ho PKH, Sirringhaus H, Friend RH (2005) Nature 434:194
17. Ohmori Y, Uchida M, Muro K, Yoshino K (1991) Japan J Appl Phys 30:1941
18. Grice AW, Bradley DDC, Bernius MT, Inbasekaran M, Wu WW, Woo EP (1998) Appl Phys Lett 73:629
19. Nakazawa YK, Carter SA, Nothofer HG, Scherf U, Lee VY, Miller RD, Scott JC (2002) Appl Phys Lett 80:3832
20. Lee JH, Hwang DH (2003) Chem Commun, p 2836
21. Yu WL, Pei J, Huang W, Heeger AJ (2000) Adv Mater 12:828
22. Wu Y, Li J, Fu Y, Bo Z (2004) Org Lett 6:3485
23. Vak D, Chun C, Lee CL, Kim JJ, Kim DY (2004) J Mater Chem 14:1342
24. Muller CD, Falcou A, Reckefuss N, Rojahn M, Wiederhirn V, Rudati P, Frohne H, Nuyen O, Becker H, Meerholz K (2003) Nature 421:829
25. Li Y, Ding J, Day M, Tao Y, Lu J, D'iorio M (2004) Chem Mater 16:2165
26. Ego C, Grimsdale AC, Uckert F, Yu G, Srdanov G, Müllen K (2002) Adv Mater 14:809
27. Chen XW, Liao JL, Liang YM, Ahmed MO, Tseng HE, Chen SA (2003) J Am Chem Soc 125:636
28. Liao JL, Chen X, Liu CY, Chen SA, Su CH, Su AC (2007) J Phys Chem B 111:10379
29. Miteva T, Meisel A, Knoll W, Nothofer HG, Scherf U, Müller DC, Meerholz K, Yasuda A, Neher D (2001) Adv Mater 13:565
30. Liu MS, Jiang X, Herguth P, Jen AKY (2001) Chem Mater 13:3820
31. Wu FI, Reddy DS, Shu CF, Liu MS, Jen AKY (2003) Chem Mater 15:269
32. Su HJ, Wu FI, Su CF, Tung YL, Chi Y, Lee GH (2005) J Polym Sci A 43:859
33. Hung MC, Liao JL, Chen SA, Chen SH, Su AC (2005) J Am Chem Soc 127:14576
34. Shu CF, Dodda R, Wu FI, Liu MS, Jen AKY (2003) Macromolecules 36:6698
35. Wu FI, Shih PI, Shu CF, Tung YL, Chi Y (2005) Macromolecules 38:9028
36. Chen YC, Huang GS, Hsiao CC, Chen SA (2006) J Am Chem Soc 128:8549

37. Yuan MC, Shih PI, Chien CH, Shu CF (2007) J Polym Sci A 45:2925
38. Chien CH, Shih PI, Wu FI, Shu CF, Chi YJ (2007) Polym Sci A 45:2073
39. Chen SH, Chou HL, Su AC, Chen SA (2004) Macromolecules 37:6833
40. Chen SH, Su AC, Chu SU, Chen SA (2005) Macromolecules 38:379
41. Chen SH, Su AC, Chen SA (2005) J Phys Chem B 109:10067
42. Ariu M, Lidzey DG, Bradley DDC (2000) Synth Met 111/112:607
43. Apperloo JJ, Janssen RAJ, Malenfant PRL, Frechet JMJ (2000) Macromolecules 33:7038
44. Grell M, Bradley DDC, Ungar G, Hill J, Whitehead KS (1999) Macromolecules 32:5810
45. Lu HH, Liu CY, Chang CH Chen SA (2007) Adv Mater 19:2574
46. Chunwaschirasiri W, Tanto B, Huber DL, Winokur MJ (2005) Phys Rev Lett 94:107402
47. Lu HH, Liu CY, Jen TH, Liao JL, Tseng HE, Huang CW, Hung MC, Chen SA (2005) Macromolecules 38:10829
48. Prieto I, Teetsov J, Fox MA, Bout DAV, Bard AJ (2001) J Phys Chem A 105:520
49. Weinfurtner KH, Fujikawa H, Tokito S, Taga Y (2000) Appl Phys Lett 76:2502
50. Chen X, Tseng HE, Liao JL, Chen SA (2005) J Phys Chem B 109:17496
51. Bliznyuk VN, Carter SA, Scott JC, Klärner G, Miller RD, Miller DC (1999) Macromolecules 32:361
52. Lee JI, Klaerner G, Miller RD (1999) Chem Mater 11:1083
53. List EJW, Guentner R, Freitas PSD, Scherf U (2002) Adv Mater 14:374
54. Gaal M, List EJW, Scherf U (2003) Macromolecules 36:4236
55. Gamerith S, Gaal M, Romaner L, Nothofer HG, Güntner R, Freitas PSD, Scherf U, List EJW (2003) Synth Met 139:855
56. Bernius MT, Inbasekaran M, O'Brien J, Wu W (2000) Adv Mater 12:1737
57. Pei J, Yu WL, Huang W, Heeger AJ (2000) Chem Commun, p 1631
58. Hou Q, Xu Y, Yang W, Yuan M, Peng J, Cao Y (2002) J Mater Chem 12:2887
59. Lim E, Jung BJ, Shim HK (2003) Macromolecules 36:4288
60. Liu MS, Luo J, Jen AKY (2003) Chem Mater 15:3496
61. Ego C, Marsitzky D, Becker S, Zhang J, Grimsdale AC, Müllen K, MacKenzie JD, Silva C, Friend RH (2003) J Am Chem Soc 125:437
62. Cho NS, Hwang DH, Jung BJ, Lim E, Lee J, Shim HK (2004) Macromolecules 37:5265
63. Wu W, Inbasekaran M, Hudack M, Welsh D, Yu W, Cheng Y, Wang C, Kram S, Tacey M, Bernius M, Fletcher R, Kiszka K, Munger S, O'Brien J (2004) Microelectron J 35:343
64. Sandee AJ, Williams CK, Evans NR, Davies JE, Boothby CE, Köhler A, Friend RH, Holmes AB (2004) J Am Chem Soc 126:7041
65. Zhang K, Chen Z, Yang C, Gong S, Qin J, Cao Y (2006) Macromol Rapid Commun 27:1926
66. Kim JH, Herguth P, Kang MS, Jen AKY, Tseng YH, Shu CF (2004) Appl Phys Lett 85:1116
67. Peng KY, Huang CW, Liu CY, Chen SA (2007) Appl Phys Lett 91:093502
68. Buchhauser D, Scheffel M, Rogler W, Tschamber C, Heuser K, Hunze A, Gieres G, Henseler D, Jakowetz W, Diekmann K, Winnacjer A, Becjer H, Busing A, Falcou A, Rau L, Vogele S, Gottling S (2004) Proc SPIE 5519:70
69. Chuang CY, Shih PI, Chien CH, Wu FI, Shu CF (2007) Macromolecules 40:247
70. Wu FI, Yang XH, Neher D, Dodda R, Tseng YH, Shu CF (2007) Adv Funct Mater 17:1085
71. He Y, Gong S, Hattori R, Kanicki J (1999) Appl Phys Lett 74:2265
72. Yan H, Huang Q, Cui J, Veinot JGC, Kern MM, Marks TJ (2003) Adv Mater 15:835
73. Müller CD, Braig T, Nothofer H, Arnoldi M, Grall M, Scherf U, Nuyken O, Meerholz K (2000) Chem Phys Chem 1:207

74. Ho PKH, Kim JS, Burroughes JH, Becker H, Li SFY, Brown TM, Cacialli F, Friend RH (2000) Nature 404:481
75. Chang CH, Liao JL, Hung MC, Chen SA (2007) Appl Phys Lett 90:063506
76. Chang CH, Chen SA (2007) Appl Phys Lett 91:103514
77. Sotzing GA, Reynolds JR, Steel PJ (1997) Adv Mater 9:795
78. Xing KZ, Fahlman M, Chen XW, Inganäs O, Salancek WR (1997) Synth Met 89:161
79. Hsiao CC, Chang CH, Lu HH, Chen SA (2007) Org Electron 8:343
80. Brown TM, Friend RH, Millard IS, Lacey DJ, Butler T, Burroughes JH, Cacialli F (2003) J Appl Phys 93:6159
81. Brown TM, Friend RH, Millard IS, Lacey DJ, Burroughes JH, Cacialli F (2001) Appl Phys Lett 79:174
82. Chan MY, Lai SL, Fung MK, Lee CS, Lee ST (2004) J Appl Phys 95:5397
83. Xu Q, Ouyang J, Yang Y, Ito T, Kido J (2003) Appl Phys Lett 83:4695
84. Huang J, Li G, Wu E, Xu Q, Yang Y (2006) Adv Mater 18:114
85. Huang J, Xu Z, Yang Y (2007) Adv Funct Mater 17:1966
86. Hsiao CC, Hsiao AE, Chen SA (2008) Adv Mater DOI: 10.1002/adma.200702150